Supplementary material

Catalytic Selectivity of Rh/TiO_2 Catalyst in Syngas Conversion to Ethanol: Probing into the Mechanism, Functions of Support TiO_2 and Promoter

Riguang Zhang Mao Peng Baojun Wang*

Key Laboratory of Coal Science and Technology of Ministry of Education and Shanxi Province, Taiyuan University of Technology, Taiyuan 030024, Shanxi, P.R. China

Part 1. All possible structures of Pt heptamer clusters, Stable configurations of the adsorbed species, and the potential energy profile of CH_x(x=1~3) and CH_3OH formation.

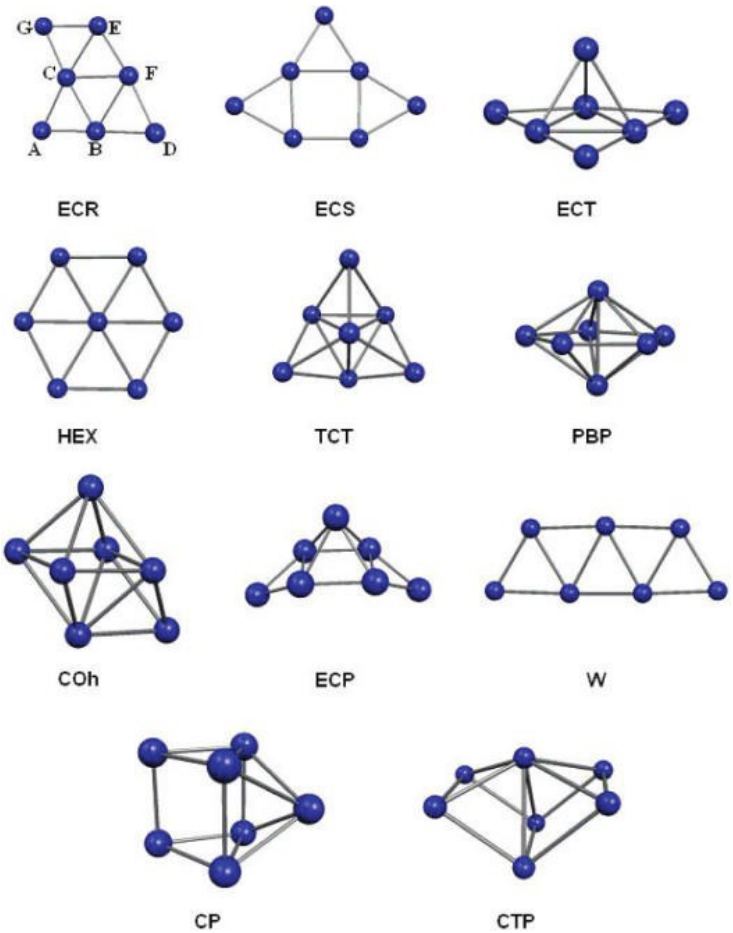

Figure S1 Structures of Rh heptamer clusters

* Corresponding author at: No. 79 Yingze West Street, Taiyuan 030024, China. Tel.: +86 351 6018239; Fax: +86 351 6041237 E-*mail address*: quantumtyut@126.com; wangbaojun@tyut.edu.cn (Baojun Wang)

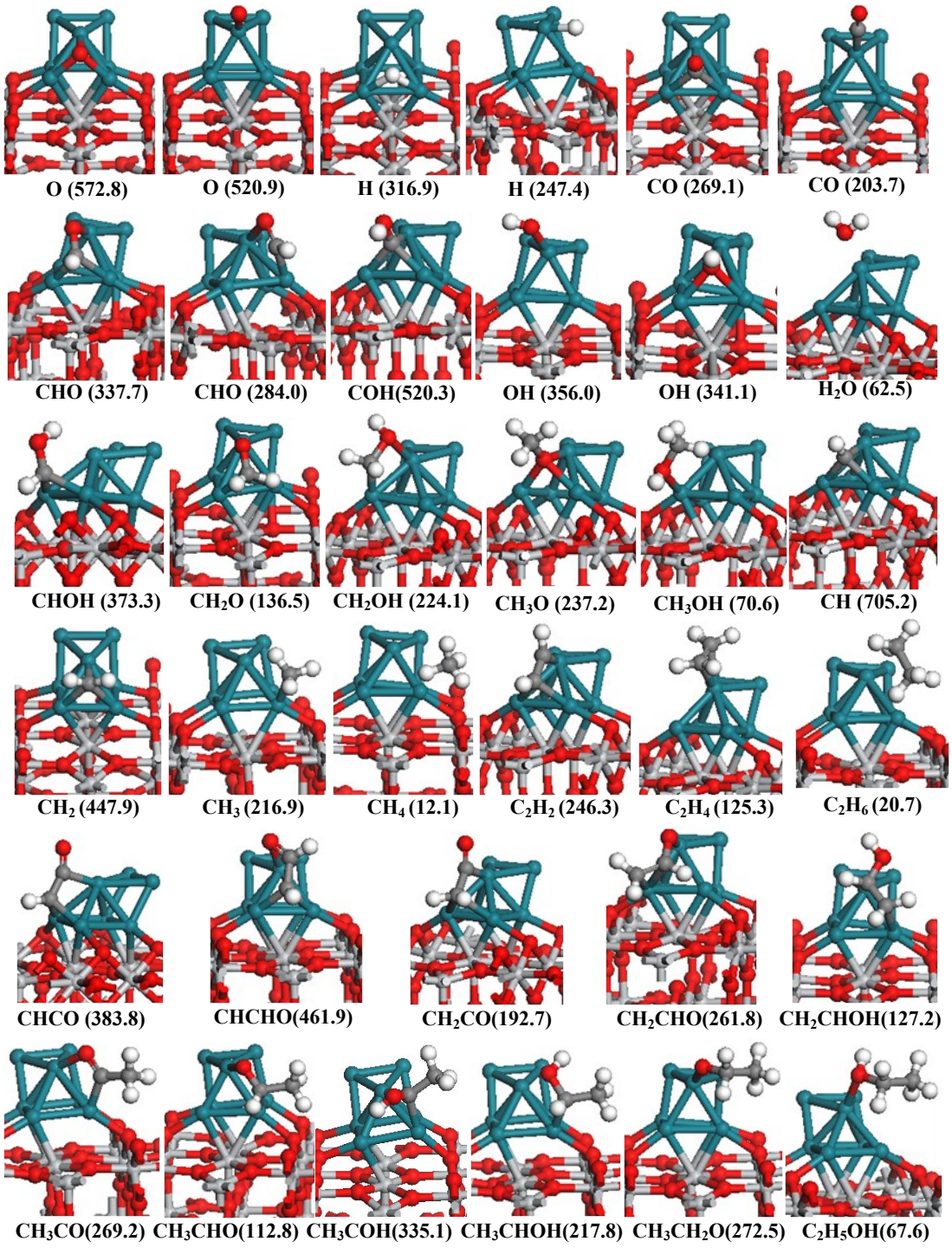

Figure S2 The stable configurations and adsorption energies of all possible species involved in ethanol synthesis from syngas. C, O, H, Ti and Rh atoms are shown in the grey, red, white, light grey and dark cyan balls, respectively. The values in parenthesis are adsorption energies with the unit in kJ·mol^{-1}.

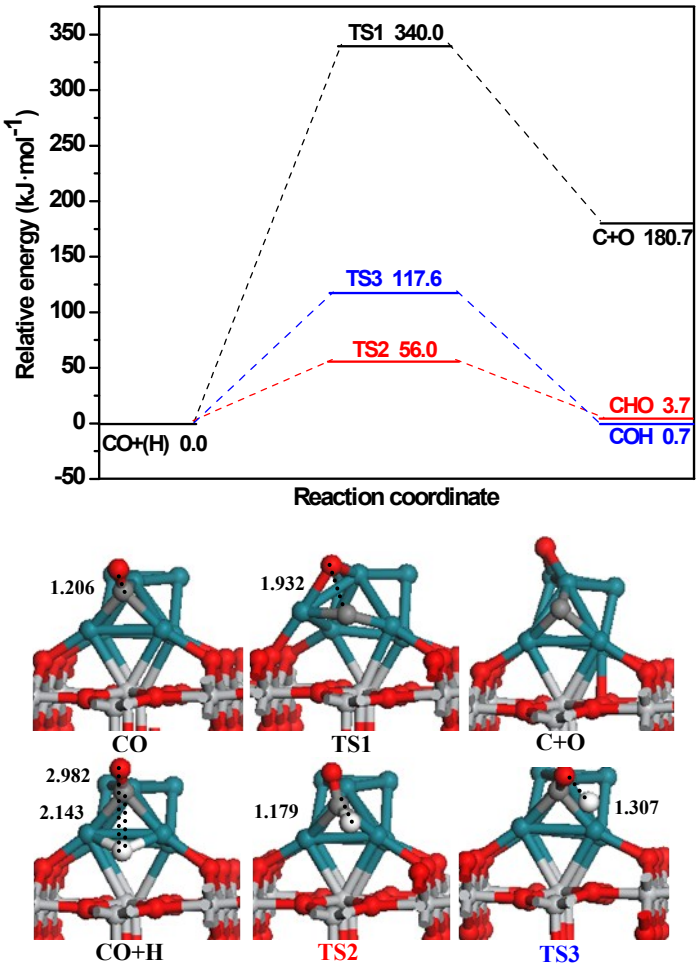

Figure S3 The potential energy profile of CO initial step together with initial states (ISs), transition states (TSs) and final states (FSs). Bond lengths are in Å. See Figure S2 for color coding.

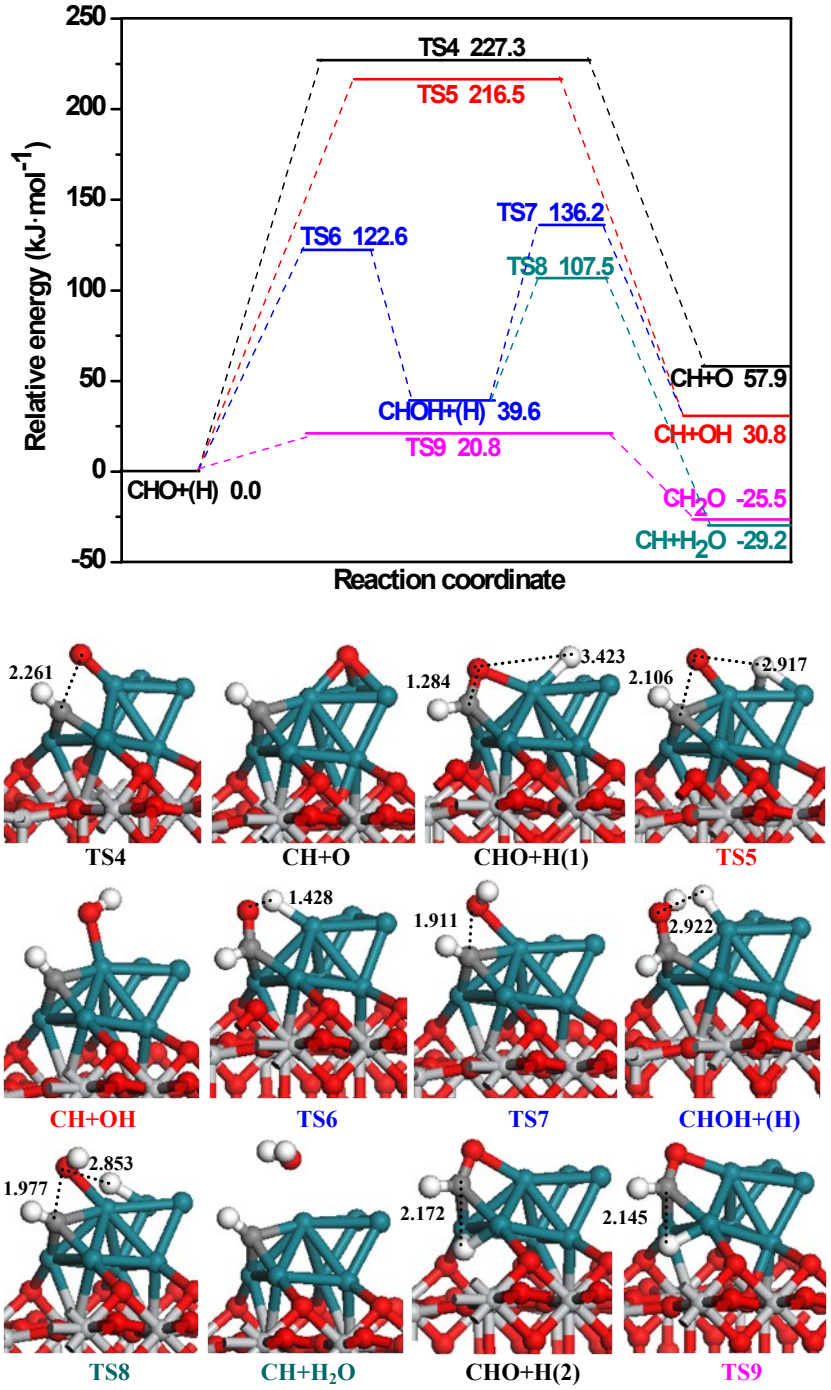

Figure S4 The potential energy profile of CH and CH_2O formations together with ISs, TSs and FSs. Bond lengths are in Å. See Figure S2 for color coding.

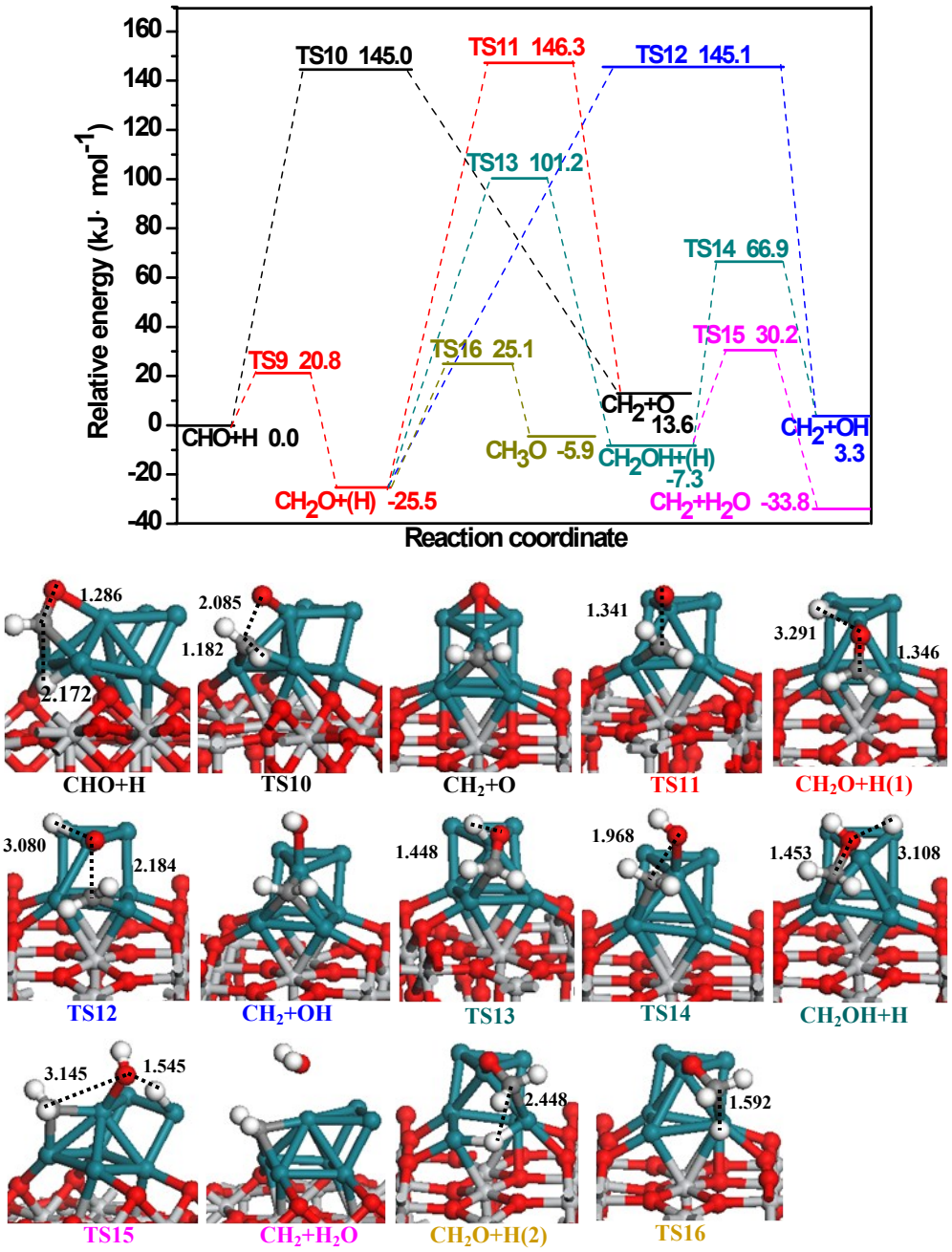

Figure S5 The potential energy profile of CH_2 and CH_3O formations together with ISs, TSs and FSs. Bond lengths are in Å. See Figure S2 for color coding.

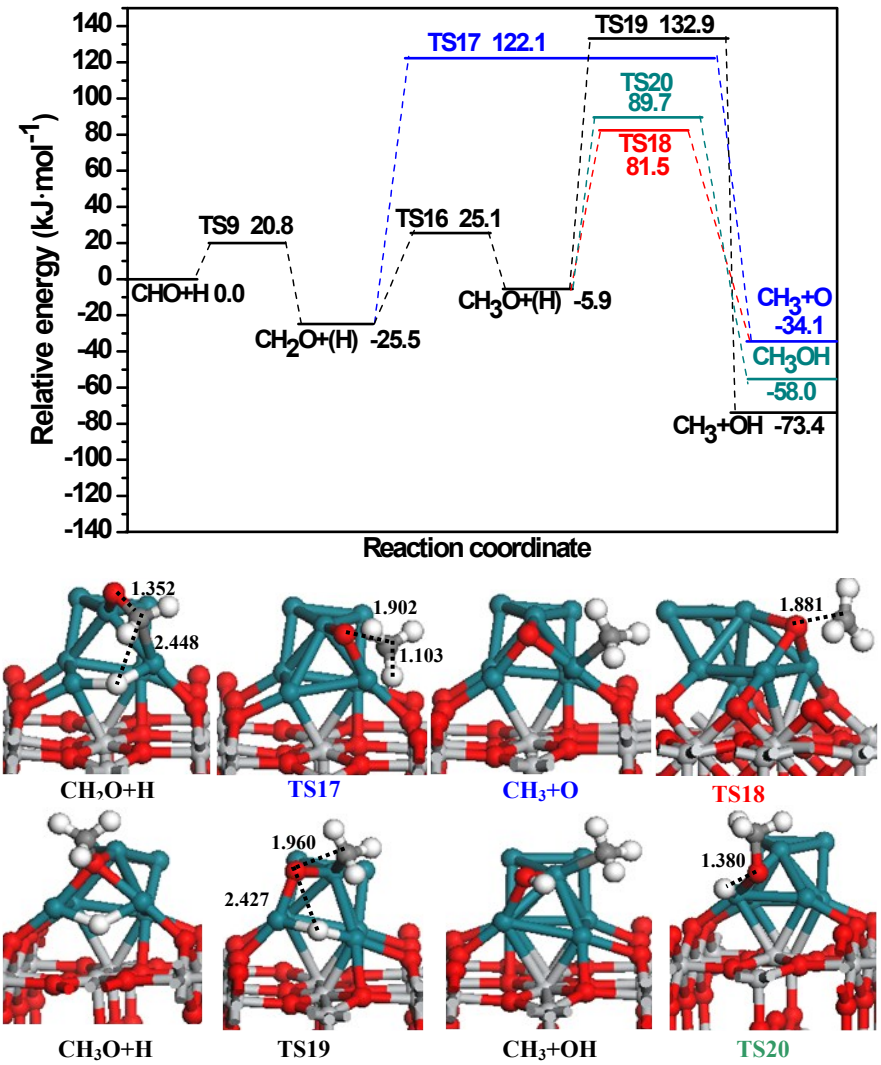

Figure S6 The potential energy profile of CH_3 and CH_3OH formations together with ISs, TSs and FSs. Bond lengths are in Å. See Figure S2 for color coding.

Part 2. The reactions related to CH_2 and CH species, as well as ethanol formation

As mentioned in the main text, due to easy formation of CH_2 by CH_3 dissociation, all reactions related to CH_2 species (**R26-R30**) have been investigated (see Figure S7), our results show that starting from CH_2 species, CH_2 hydrogenation to CH_3 is the most favorable, which have the activation energy and reaction energy of 24.1 and -11.2 kJ·mol^{-1}, respectively; the second is CH_2 dissociation to CH, which have the activation energy and reaction energy of 40.1 and 26.6 kJ·mol^{-1}, respectively; the third is CHO insertion into CH_2 to CH_2CHO, which have the activation energy and reaction energy of 84.0 and -8.0 kJ·mol^{-1}, respectively.

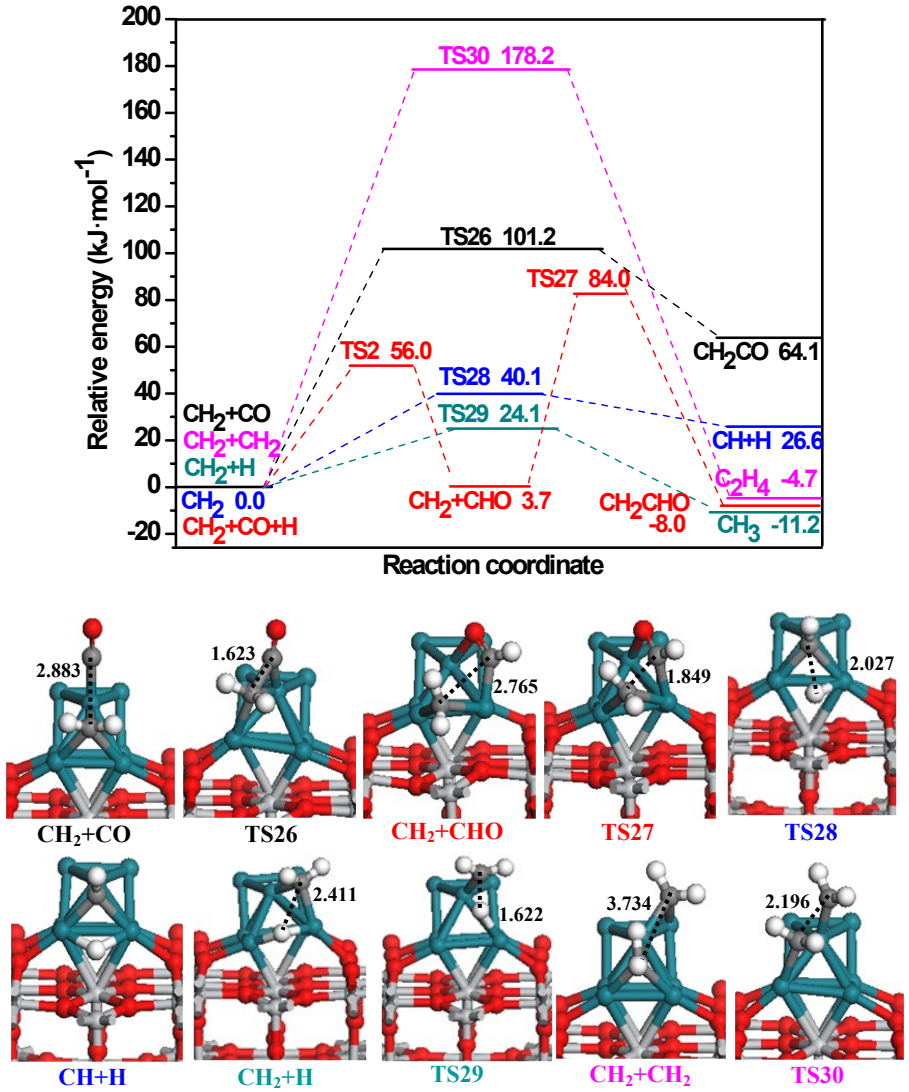

Figure S7 The potential energy profile of these reactions related to CH_2 species together with ISs, TSs and FSs. Bond lengths are in Å. See Figure S2 for color coding in the main text.

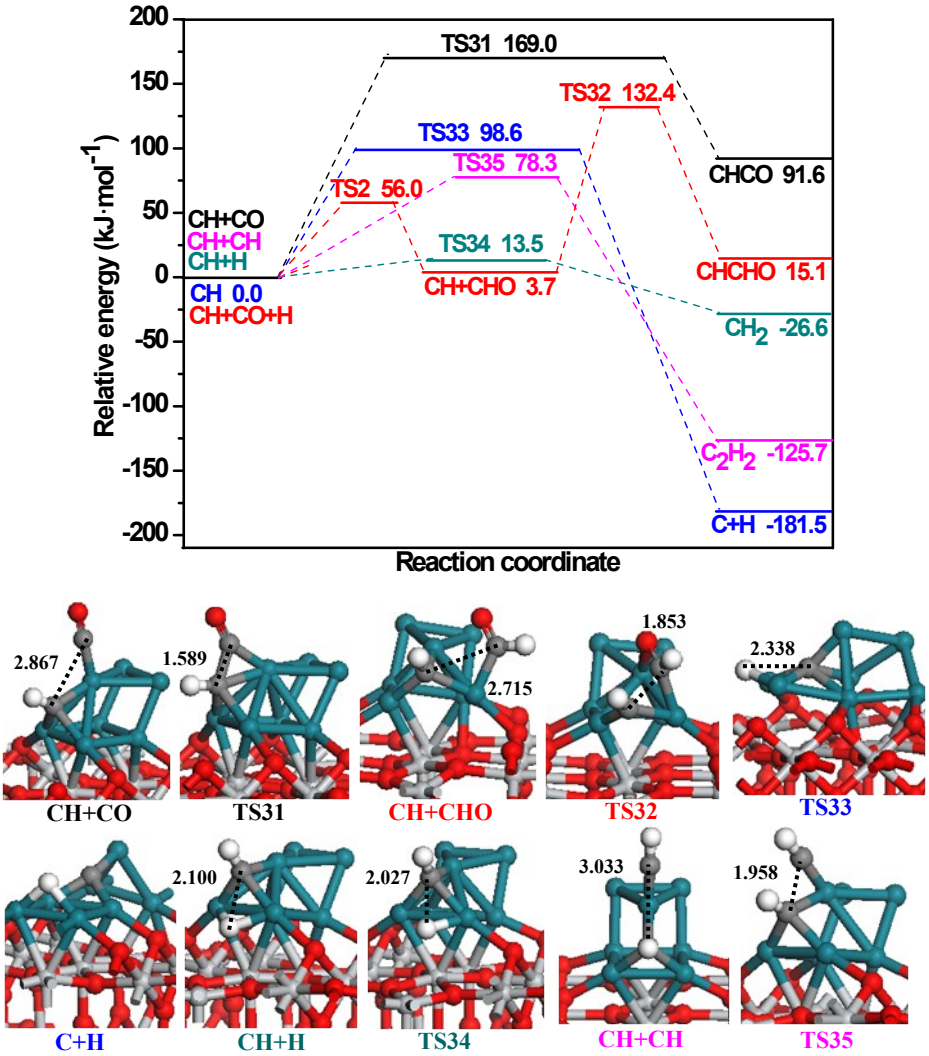

Figure S8 The potential energy profile of these reactions related to CH species together with ISs, TSs and FSs. Bond lengths are in Å. See Figure S2 for color coding in the main text.

On the other hand, all reactions related to CH species (**R31-R35**) have also been examined (see Figure S8), suggesting that CH prefers to be hydrogenated to CH_2, which have the activation energy and reaction energy of 13.5 and -26.6 kJ·mol^{-1}, respectively; the second is CH coupling, which have the activation energy and reaction energy of 78.3 and -125.7 kJ·mol^{-1}, respectively; CHO or CO insertion into CH to C_2 oxygenates are difficult to occur.

Further, it is noted that starting from CH_3 species, CH and CH_2 can be easily formed, however, among all reactions related to CH and CH_2 species, CH and CH_2 prefers to be hydrogenated to CH_2 and CH_3, respectively, which means that once CH and CH_2 species are formed, both prefer to be

hydrogenated to CH_3. Therefore, CH_3 species is the most favorable CH_x monomer on Rh/TiO_2 catalyst, which is dominantly responsible for C_2 oxygenates formation.

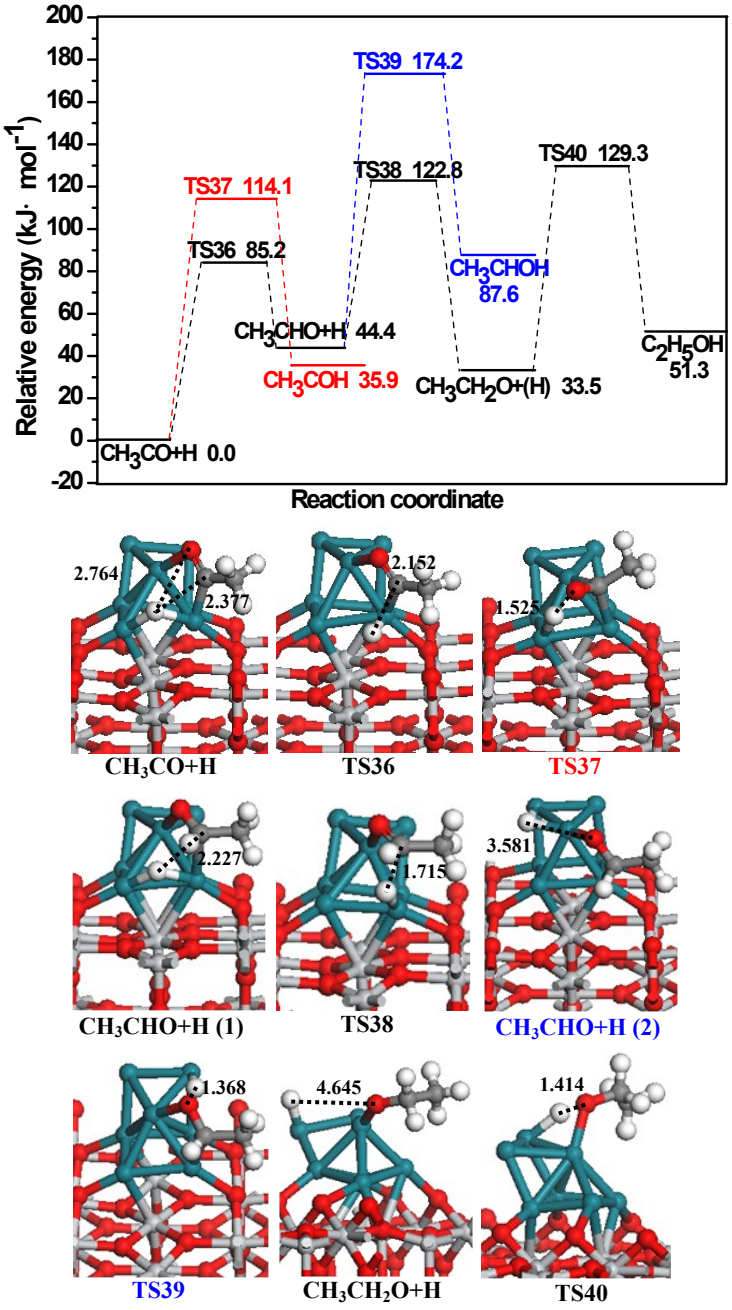

Figure S9 The potential energy profile of ethanol formation starting from CH_3CO successive hydrogenation together with ISs, TSs and FSs. Bond lengths are in Å. See Figure 2 for color coding.

Part 3. Rate constant calculations

In this study, the rate constants of all elementary reactions involved in ethanol synthesis from syngas at different temperatures have been calculated to further understand the effect of reaction

temperature on the kinetic of ethanol, methanol and methane formations on Rh/TiO_2 catalyst. Previous studies has reported that Rh-based catalysts exhibit a good catalytic activity toward C_2 oxygenates, where the reaction temperature ranges from 563 to 593 K.[1-3] Hence, the rate constants of all elementary reactions at T=500, 525, 550, 575, 600, 625 K have been considered, respectively.

On the basis of the harmonic Transition State Theory (TST), the rate constant can be obtained using the Eq. (1):[4,5]

$$k=\frac{k_B T}{h}\frac{q_{TS}}{q_{React}}\exp\left(-\frac{E_a}{RT}\right) \qquad (1)$$

Here k_B is the Boltzmann constant, h is the Planck constant, T is the absolute temperature, E_a is the zero-point-corrected energy difference between the transition state and the co-adsorbed reactants. The partition functions (q) are calculated in the harmonic model in Eq. (2), where v is the vibrational frequency.

$$q=\frac{1}{\sum_{i=1}^{Vibrations} 1-\exp\left(-\frac{h\nu_i}{k_B T}\right)} \qquad (2)$$

The zero-point-corrected activation energy (E_a) is determined from Eqs. (3) and (4):[5,6]

$$E_a = (E_{TS} - E_{IS}) + \Delta ZPE_{barrier} \qquad (3)$$

Where E_{TS} corresponds to the TS energy, E_{IS} refers to the reactant energy, and $\Delta ZPE_{barrier}$ refers to ZPE correction. For the co-adsorbed reactants, the reactant energy (E_{IS}) is calculated as the sum of individual BEs. ZPE correction for the activation energy is determined from the Eq. (4).

$$\Delta ZPE_{barrier}=\left(\sum_{i=1}^{Vibrations}\frac{h\nu_i}{2}\right)_{TS}-\left(\sum_{i=1}^{Vibrations}\frac{h\nu_i}{2}\right)_{IS} \qquad (4)$$

Aiming at providing more accurate energies for the kinetic modeling, the activation energy with ZPE-corrected has been considered, which vary slightly from those without ZPE-corrected. According to above formulas, the rate constants of all elementary reaction involved in ethanol from syngas have been calculated, and the corresponding results are listed in Table S1.

Table S1 The partial elementary reactions involved in ethanol synthesis from syngas together with the ZPE-corrected activation energies (E_a') and rate constants.

Elementary reactions	E_a'/(kJ/mol)		Rate constant (T/K)					
			500	525	550	575	600	625
CO+H→CHO	57.6	k_1	1.44×10^{7}	2.94×10^{7}	5.67×10^{7}	1.03×10^{8}	1.79×10^{8}	2.98×10^{8}
CHO+H→CH_2O	20.1	k_2	7.82×10^{10}	1.04×10^{11}	1.36×10^{11}	1.73×10^{11}	2.17×10^{11}	2.68×10^{11}
CH_2O+H→CH_3O	51.2	k_3	4.02×10^{7}	7.63×10^{7}	1.37×10^{8}	2.34×10^{8}	3.84×10^{8}	6.06×10^{8}
CH_3O→CH_3+O	80.5	k_4	6.59×10^{4}	1.79×10^{5}	4.45×10^{5}	1.03×10^{6}	2.22×10^{6}	4.52×10^{6}
CH_3O+H→CH_3OH	94.7	k_5	4.24×10^{3}	1.33×10^{4}	3.79×10^{4}	9.84×10^{4}	2.37×10^{5}	5.32×10^{5}
CH_3+CO→CH_3CO	108.2	k_6	3.39×10^{1}	1.21×10^{2}	3.86×10^{2}	1.11×10^{3}	2.94×10^{3}	7.21×10^{3}
CH_3+H→CH_4	74.8	k_7	2.40×10^{5}	5.97×10^{5}	1.37×10^{6}	2.94×10^{6}	5.92×10^{6}	1.13×10^{7}
CH_3CO+H→CH_3CHO	82.4	k_8	2.30×10^{4}	6.26×10^{4}	1.56×10^{5}	3.59×10^{5}	7.74×10^{5}	1.57×10^{5}
CH_3CHO+H→CH_3CH_2O	76.7	k_9	2.91×10^{4}	7.43×10^{4}	1.75×10^{5}	3.83×10^{5}	7.89×10^{5}	1.53×10^{6}
CH_3CH_2O+H→C_2H_5OH	100.3	k_{10}	1.34×10^{3}	4.38×10^{3}	1.29×10^{4}	3.47×10^{4}	8.58×10^{4}	1.98×10^{5}
O+H→OH	62.8	k_{11}	3.44×10^{6}	7.48×10^{6}	1.52×10^{7}	2.92×10^{7}	5.31×10^{7}	9.22×10^{7}
OH+H→H_2O	99.4	k_{12}	5.75×10^{2}	1.89×10^{3}	5.62×10^{3}	1.52×10^{4}	3.78×10^{4}	8.76×10^{4}

Part 4. Microkinetic Modeling

In this study, the microkinetic modeling technique has been employed to investigate the catalytic activity and selectivity of major products in ethanol synthesis from syngas on Rh/TiO_2 catalyst, in which the method applied has been widely employed in the previous studies.[2,7,8] The adsorption process of syngas is assumed to be in equilibrium. Meanwhile, all elementary reactions involved in the microkinetic modeling have been summarized in Table S1.

For the microkinetic modeling in syngas conversion, the adsorption processes of CO and H_2 are assumed to be in equilibrium. Moreover, the pseudo-steady-state approximation[8] is applied to other minority species on the catalyst surface, namely, the production rates and the consumption rates of all species involved are thought to be the same. The equilibrium constants for H_2 and CO adsorption are estimated according to the formula:

$$K = \exp[-(\Delta E_{ads} - T\Delta S)/RT] \quad (5)$$

Here ΔE_{ads} is the adsorption energy of adsorbate, ΔS is the entropy change of gas-phase adsorbate, which can be obtained from NIST Chemistry WebBook.[9] While R is the fundamental gas constant, T is the reaction temperature.

The site balance of all intermediate species involved in the reaction mechanism can be described in terms of coverage (θ_x, x=surface species), as presented in Eq. (6):

$$\theta_{CO} + \theta_H + \theta_{CHO} + \theta_{CH_2O} + \theta_{CH_3O} + \theta_{CH_3} + \theta_{CH_3CO} + \theta_{CH_3CHO} + \theta_{CH_3CH_2O} + \theta_O + \theta_{OH} + \theta_* = 1 \quad \textbf{(6)}$$

The coverage of H_2 and CO are $\theta_H=(P_{H_2}K_2)^{1/2}\theta_*$ and $\theta_{CO}=P_{CO}K_3\theta_*$, respectively. Other involved surface species can be described according to the steady-state approximation as summarized below,[8] where the rates of production and consumption are considered to be the same.

CO: $\theta_{CO} = P_{CO}K_1\theta_*$

H: $\theta_H = P_{H_2}^{1/2}K_2^{1/2}\theta_*$

CHO: $\frac{d\theta_{CHO}}{dt} = k_1\theta_{CO}\theta_H - k_2\theta_{CHO}\theta_H = 0$

CH_2O: $\frac{d\theta_{CH_2O}}{dt} = k_2\theta_{CHO}\theta_H - k_3\theta_{CH_2O}\theta_H = 0$

CH_3O: $\frac{d\theta_{CH_3O}}{dt} = k_3\theta_{CH_2O}\theta_H - k_4\theta_{CH_3O}\theta_* - k_5\theta_{CH_3O}\theta_H = 0$

CH_3: $\frac{d\theta_{CH_3}}{dt} = k_4\theta_{CH_3O}\theta_* - k_6\theta_{CH_3}\theta_{CO} - k_7\theta_{CH_3}\theta_H = 0$

CH_3CO: $\frac{d\theta_{CH_3CO}}{dt} = k_6\theta_{CH_3}\theta_{CO} - k_8\theta_{CH_3CO}\theta_H = 0$

CH_3CHO: $\frac{d\theta_{CH_3CHO}}{dt} = k_8\theta_{CH_3CO}\theta_H - k_9\theta_{CH_3CHO}\theta_H = 0$

CH_3CH_2O: $\frac{d\theta_{CH_3CH_2O}}{dt} = k_9\theta_{CH_3CHO}\theta_H - k_{10}\theta_{CH_3CH_2O}\theta_H = 0$

O: $\frac{d\theta_O}{dt} = k_4\theta_{CH_3O}\theta_* - k_{11}\theta_O\theta_H = 0$

OH: $\frac{d\theta_{OH}}{dt} = k_{10}\theta_O\theta_H - k_{12}\theta_{OH}\theta_H = 0$

Putting all of the coverage expressions into Eq. (6), the coverage of surface free sites θ_* can be obtained. Subsequently, the coverage of every adsorbates can be obtained.

In ethanol synthesis from syngas on Rh/TiO_2 catalyst, CO→CHO→CH_2O→CH_3O is an optimal pathway for initial CO hydrogenation; starting from CH_3O intermediate, CH_3OH formation goes through CH_3O hydrogenation, CH_3 is formed by CH_3O dissociation. Starting from CH_3 species, CH_4 is formed by its hydrogenation, while CO insertion into CH_3 is the favorable pathway to form C_2 oxygenate CH_3CO, which will be successively hydrogenated to ethanol; moreover, CO insertion into CH_3 to CH_3CO is the rate-controlling step of ethanol formation, as a result, the rates of C_2H_5OH formation is determined by CO insertion into CH_3 to CH_3CO.

The rates for the major products CH_3OH, CH_4 and C_2H_5OH are:

$$r_{CH_3OH} = k_5\theta_{CH_3O}\theta_H$$

$$r_{CH_4} = k_7\theta_{CH_3}\theta_H$$

$$r_{C_2H_5OH} \approx r_{CH_3CO} = k_6\theta_{CH_3}\theta_{CO}$$

The relative selectivity is defined by the relative rate for each product, as mentioned below, in which *i* is CH_3OH, CH_4 or C_2H_5OH:

$$s_i = r_i / (r_{CH_3OH} + r_{CH_4} + r_{C_2H_5OH})$$

Part 5. The Role of Promoter Fe for Fe-promoted Rh/TiO_2 Catalyst

Since Fe has been widely used in experiments as one of the promoters for ethanol synthesis from syngas on Rh-based catalyst,[2,10-13] to further validate above predictions about the role of promoter, one example has been carried out to probe into the effect of promoter Fe on Fe-promoted Rh/TiO_2 catalyst.

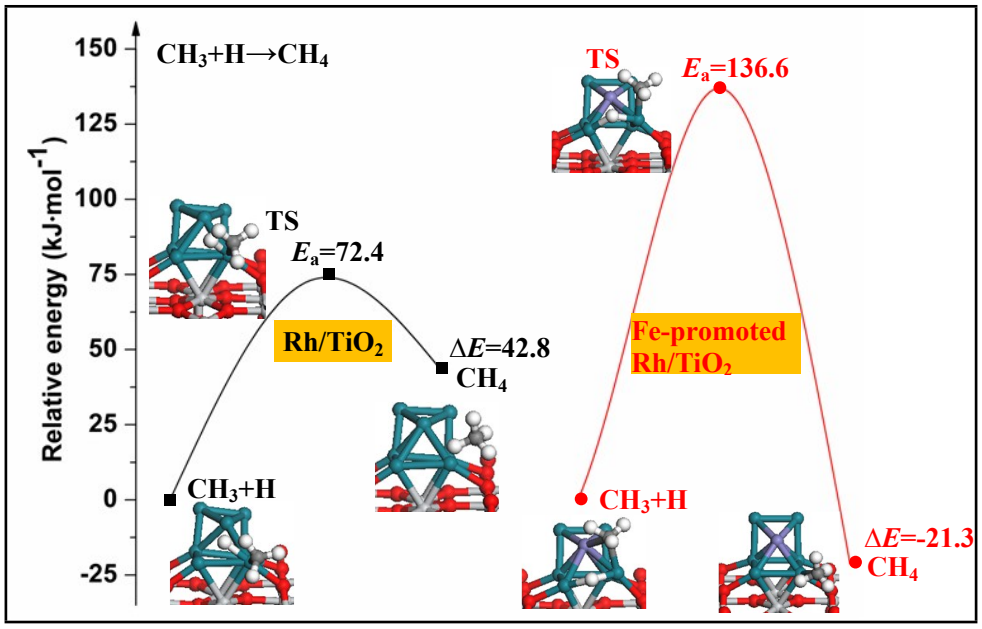

Figure S10 Comparisons of activation energies (E_a/kJ·mol^{-1}) and reaction energies (ΔE/kJ·mol^{-1}) for CH_4 formation by CH_3 hydrogenation on Rh/TiO_2 and Fe-promoted Rh/TiO_2 catalysts, respectively.

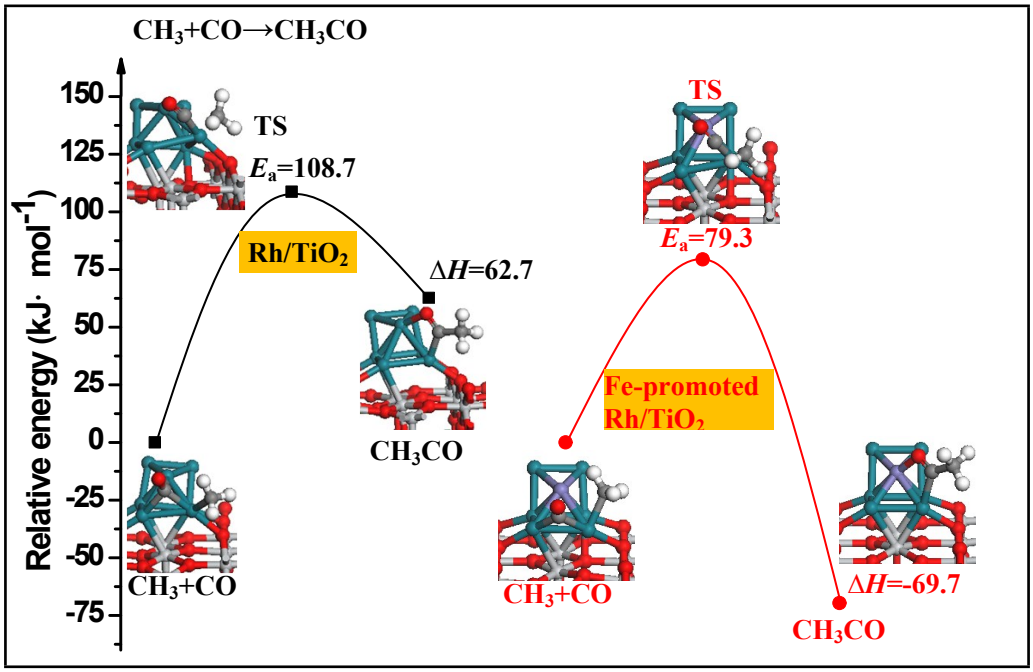

Figure S11 Comparisons of activation energies (E_a/kJ·mol^{-1}) and reaction energies (ΔH/kJ·mol^{-1}) for CH_3CO formation by CO insertion into CH_3 on Rh/TiO_2 and Fe-promoted Rh/TiO_2 catalysts, respectively.

In this study, Fe is occupied as the promoter of Rh/TiO_2 catalyst; for Fe-promoted Rh/TiO_2 model catalyst, two types of models may exist: one is to replace a Rh atom from the topmost layer of Rh_7 nanocluster by a Fe atom, as shown in Figures S10 and S11; the other is to adsorb a Fe atom

onto Rh_7 nanocluster. Nowadays, extensive studies about the effect of promoter on C_2 oxygenates formation from syngas mainly focus on the first type of model.[2,14-17] Thus, only the first model with a Rh atom from the topmost layer of Rh_7 nanocluster replaced by a Fe atom has been considered as the promoter Fe-promoted Rh/TiO_2 catalyst model in this study.

Our results show that on Fe-promoted Rh/TiO_2 catalyst, CH_4 formation by CH_3 hydrogenation is exothermic by 21.3 $kJ \cdot mol^{-1}$ with an activation energy of 136.6 $kJ \cdot mol^{-1}$, which is much higher than that on Rh/TiO_2 catalyst by 64.2 $kJ \cdot mol^{-1}$, suggesting that the promoter Fe can suppress CH_4 formation upon going from Rh/TiO_2 to Fe-promoted Rh/TiO_2 catalyst (see Figure S10).

Interestingly, CO insertion into CH_3 to CH_3CO on Fe-promoted Rh/TiO_2 catalyst is exothermic by 69.7 $kJ \cdot mol^{-1}$ with an activation energy of 79.3 $kJ \cdot mol^{-1}$, which is much higher than that on Rh/TiO_2 catalyst by 29.4 $kJ \cdot mol^{-1}$, indicating that the promoter Fe can promote CH_3CO formation upon going from Rh/TiO_2 to Fe-promoted Rh/TiO_2 catalyst (see Figure S11). Thus, the effect of promoter Fe is very sensitive to CH_4 and CH_3CO formations.

Part 6. Density of States of Rh_7/TiO_2 and $FeRh_6/TiO_2$ Catalysts, as well as the Adsorbed Species Involving in the Reactions of CH_3 Hydrogenation and CO Insertion into CH_3

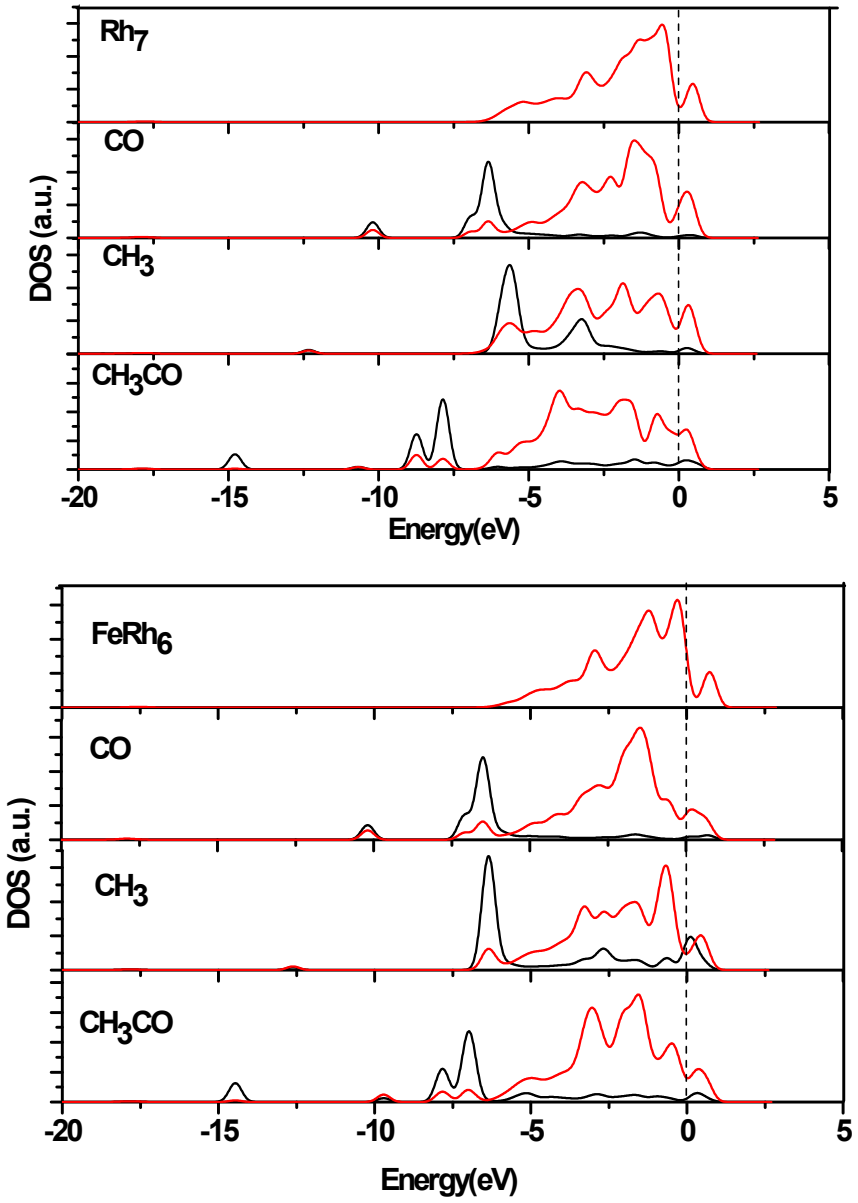

Figure S12 Density of states for bare Rh atoms of Rh_7/TiO_2 and $FeRh_6/TiO_2$, as well as the adsorbed CO, CH_3, and CH_3CO species on Rh_7/TiO_2 and $FeRh_6/TiO_2$. The red lines denote *d*-orbital of Rh atom in Rh_7/TiO_2 and $FeRh_6/TiO_2$, while the black lines correspond to *p*-orbital of the C atoms. The dashed line is the Fermi level.

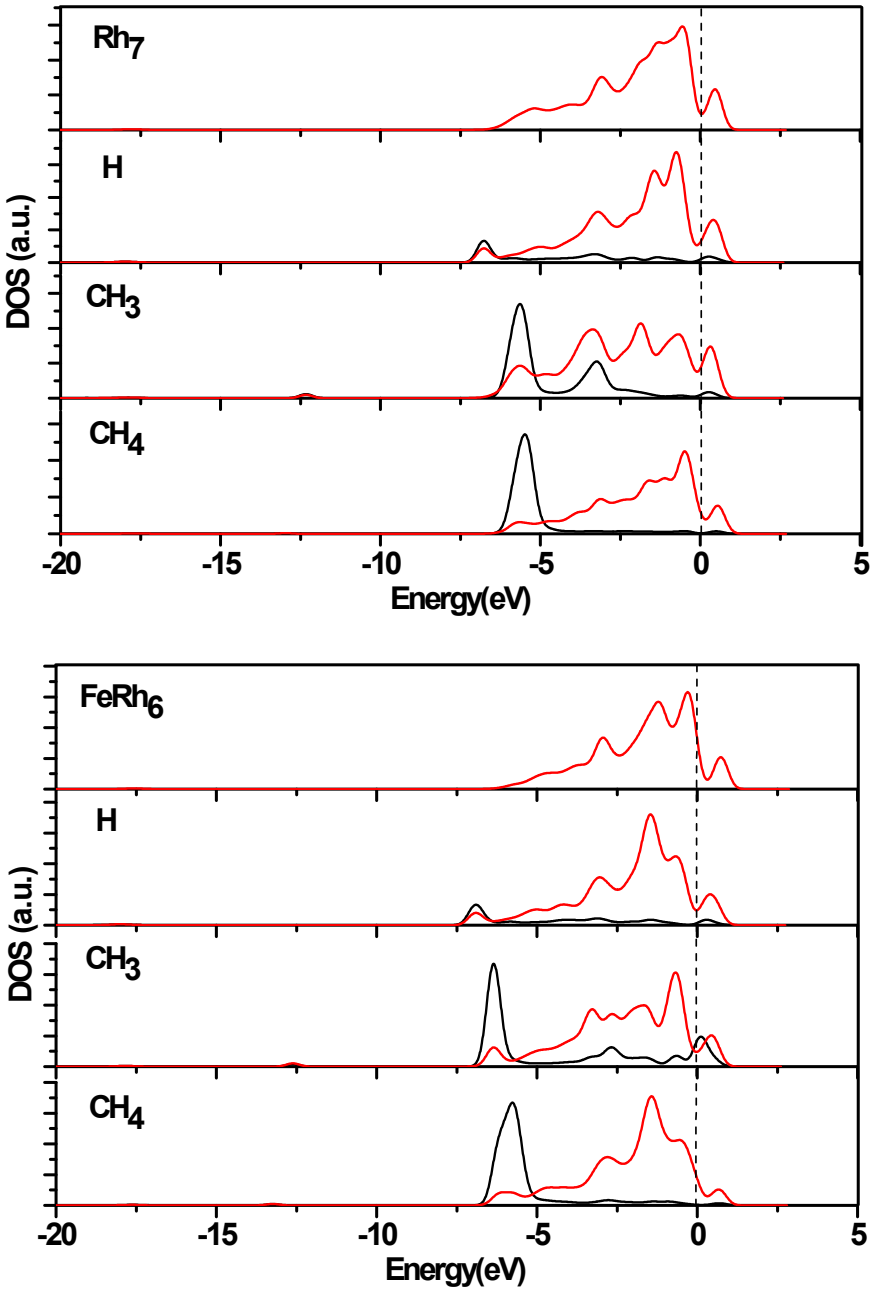

Figure S13 Density of states for bare Rh atoms of Rh_7/TiO_2 and $FeRh_6/TiO_2$, as well as the adsorbed H, CH_3, and CH_4 species on Rh_7/TiO_2 and $FeRh_6/TiO_2$. The red lines denote *d*-orbital of Rh atom in Rh_7/TiO_2 and $FeRh_6/TiO_2$, while the black lines correspond to *p*-orbital of the C atoms. The dashed line is the Fermi level.

References

[1] P.Z. Lin, D.B. Liang, H.Y. Luo, C.H. Xu, H.W. Zhou, S.Y. Huang, L.W. Lin, *Appl. Catal. A: Gen.*, 1995, **131**, 207–214.

[2] Y.M. Choi, P. Liu, *J. Am. Chem. Soc.*, 2009, **131**, 13054–13061.

[3] W.M. Chen, Y.J. Ding, D.H. Jiang, T. Wang, H.Y. Luo, *Catal. Commun.*, 2006, **7**, 559–562.

[4] J.P. Clay, J.P. Greeley, F.H. Ribeiro, W.N Delgass, W.F. Schneider, *J. Catal.*, 2014, **320**, 106−117.

[5] X. Guo, H. Liu, B. Wang, Q. Wang, R. Zhang, *RSC Adv.*, 2015, **5**, 19970−19982.

[6] N. Kapur, J. Hyun, B. Shan, J.B. Nicholas, K. Cho, *J. Phys. Chem. C.*, 2010, **114**, 10171−10182.

[7] P. Liu, J. A. Rodriguez, *J. Chem. Phys.*, 2007, **126**, 164705–164712.

[8] P. Liu, A. Logadottir, J.K. Nørskov, *Electrochim. Acta*, 2003, **48**, 3731–3742.

[9] http://webbook.nist.gov/chemistry/.

[10] V. Subramani, S.K. Gangwal, *Energy Fuels*, 2008, **22**, 814–839.

[11] J.J. Spivey, A. Egbebi, Chem. *Soc. Rev.*, 2007, **36**, 1514–1528.

[12] M.A. Haider, M.R. Gogate, R.J. Davis, *J. Catal.*, 2009, **261**, 9–16.

[13] A. Deluzarche, J.P. Hindermann, R. Kieffer, R. Breault, A. Kiennernann, *J. Phys. Chem.*, 1984, **88**, 4993–4995.

[14] R.G. Zhang, G.R. Wang, B.J. Wang, *J. Catal.*, 2013, **305**, 238–255.

[15] Y.H. Zhao, M.M. Yang, D.P. Sun, H.Y. Su, K.J. Sun, X.F. Ma, X.H. Bao, W.X. Li, *J. Phys. Chem. C*, 2011, **115**, 18247–18256.

[16] F.Y. Li, D.E. Jiang, X.C. Zeng, Z.F. Chen, *Nanoscale*, 2012, **4**, 1123–1129.

[17] R.G. Zhang, G.R. Wang, B.J. Wang, L.X. Ling, *J. Phys. Chem. C*, 2014, **11**, 85243−5254.